Int J Adv Life Sci Res. Volume 7(4) 129-145
https://doi.org/10.31632/ijalsr.2024.v07i04.012

International Journal of Advancement in Life Sciences Research

Online ISSN: 2581-4877

Journal homepage http://ijalsr.org

Original Article

CaP Scaffold Loaded with Multi-Functional Gel for Bone Repair after Resection of Osteosarcoma

Yun Cao[1,2*], Nan Yang[1], Yangyang Zheng[1], Qiang He[1], Jiahu Huang[1], Farra Aidah Jumuddin[2*]

[1]*Sichuan Science City Hospital, Mianyang 610299, P. R. China*
[2]*Faculty of Medicine, Lincoln University College, Malaysia*

**Correspondence E-mail:cdcaoyun@126.com; farraaidah@lincoln.edu.my*

Abstract

Introduction: Osteosarcoma resection in clinical settings often causes largeosteopenia, and the cancer cells at the site of the lesion easily lead to the recurrence of osteosarcoma. Therefore, the treatment of osteosarcoma should not only induce bone regeneration, and remove tumor cells from the lesion site, but also avoid bacterial infection. **Objective:** This study is to develop a multifunctional scaffold that combines chitosan, black phosphorus nanoparticles, and copper ions in a biphasic calcium phosphate matrix to enhance bone regeneration, reduce tumor recurrence, and prevent infections following osteosarcoma surgery. **Methods:** Herein, a Biphasic Calcium Phosphate (BCP) porous scaffold was prepared by the pore-forming agent method, and the mixed gel of chitosan (CS), Black Phosphorus nanoparticles (BP), and Copper ion (Cu^{2+}) was filled into the porous scaffold to form a composite scaffold (CS/BP/Cu-BCPs). CS/BP/Cu-BCPs were used to treat large bone defects caused by osteosarcoma. The composite scaffolds contain anticancer, bone promoting and bacteriostatic properties, which are mainly put down to the anticancer properties of BCP and BP, the osteoinductivity of BCP and Cu^{2+}, and the antimicrobial effects of CS and Cu^{2+}.Cell and antimicrobial tests demonstrated that the extract of CS/BP/Cu-BCPs displayed good biocompatibility, induced osteogenic differentiation of mesenchymal stem cells (BMSCs), and inhibited the growth of bacteria. **Results:** *In vivo,* experiments showed CS/BP/Cu-BCPs had obvious anti-tumor and osteogenic effects. Taken together, the CS/BP/Cu-BCPs prepared in this study possessed good functions such as oncotherapy, bone regeneration, and postoperative anti-infection, and were expected to become a simple therapeutic material for osteosarcoma resection. We investigated the *in vitro* antibacterial, *in vivo* osteogenic, and antitumor capabilities of CaP scaffolds loaded with multi-functional gels. Compared with the control group, CaP scaffolds loaded with multi-functional gel showed significant antibacterial, bone-promoting, and anti-tumor effects. **Conclusion:** The contribution of this study was to confirm that CaP scaffolds loaded with multi-functional gels could eliminate osteosarcoma while repairing critical bone defects and have good antibacterial potential. These results suggested that CaP scaffolds loaded with multifunctional gels may be a potential candidate for repairing bone defects caused by osteosarcoma resection.

Keywords: *antibacterial, bone, cell, osteosarcoma, scaffold*.

Introduction

Osteosarcoma, primarily afflicting children and adolescents, presents with dismal prognoses marked by high metastasis rates, recurrence tendencies, and poor survival rates (Kansara *et al.*, 2014; Ritter & Bielack, 2010). Despite significant advancements in molecular biology and genetics, the clinical therapeutic efficacy of osteosarcoma remains largely stagnant. Current treatments primarily rely on surgical resection and chemotherapy, albeit these interventions often lead to bone defects, chronic osteomyelitis, and severe chemotherapy-induced side effects, intensifying patient distress (Luetke *et*

Received on :12th July 2024; Revised version received on :17th September 2024; Accepted: 29th September 2024

al., 2014). Moreover, residual tumor cells post-surgery pose significant risks of local recurrence, with non-metastatic patients experiencing recurrence rates as high as 30–40% (Sanuki-Fujimoto *et al.*, 2008). Wound infections during the hemostasis process present another major challenge, potentially leading to amputation, abscess formation, or delayed healing (Cheng *et al.*, 2020; Ingley *et al.*, 2022). An ideal material for treating bone defects post-tumor removal should exhibit anti-tumor, bone-forming, and anti-infection properties.

Hydroxyapatite (HA), a natural bone constituent, exerts a pivotal role in bone mineralization and is widely utilized in orthopedic implants (Mir *et al.*, 2023). Biphasic calcium phosphate (BCP), consisting of β-Tricalcium phosphate (β-TCP) and HA, has emerged as a clinical gold standard despite its drawbacks like slow degradation rates and brittleness (Feng *et al.*, 2022). BCP, compared to HA or β-TCP, offers an adjustable degradation rate impacting bone regeneration, and BCP has become a gold standard in the clinical treatment of bone defects (Deng *et al.*, 2021). Although BCP offers an adjustable degradation rate impacting bone regeneration, it suffers from brittleness. To address this, we introduce polymers like chitosan (CS) to reinforce BCP scaffolds, enhancing their resilience. CS, derived from shrimp and crab shells, boasts excellent biocompatibility, biodegradability, and antibacterial properties, facilitating bone cell proliferation and differentiation (Duong *et al.*, 2018; Waibel *et al.*, 2011). Milos *et al.* incorporated CS and HA nanoparticles into collagen membranes, which may be conducive to promoting bone formation and reducing bacterial adhesion (Lazarevic *et al.*, 2023).

After osteosarcoma resection, removing residual tumor cells at the site of the lesion before repairing the bone defect is a key step to prevent bone tumor recurrence. Black phosphorus nanoparticles (BP) are incorporated for structural integrity and cell growth promotion due to their biocompatibility and biodegradability (Qiu *et al.*, 2019). BP also enhances the anti-tumor effect of calcium phosphate, potentially preventing osteosarcoma recurrence (Ma *et al.*, 2022). Copper ions (Cu^{2+}) are introduced for their angiogenic and antibacterial properties, essential in bone healing and infection prevention (Yao *et al.*, 2019; Zhou *et al.*, 2021).Cu^{2+} also exhibits anti-tumor effects, further enhancing the scaffold's therapeutic potential (da Silva *et al.*, 2022).Drawing from the advantageous properties of CS, BP, Cu^{2+}, and BCP, our study develops a porous CS/BP/Cu-BCP scaffold (CS/BP/Cu-BCPs) with multiple functionalities. This scaffold offers a comprehensive solution for postoperative osteosarcoma management, significantly reducing treatment costs and promoting sustainable development in medical applications.

Problem Statement

Osteosarcoma, primarily affecting children and adolescents, has poor outcomes due to high recurrence and metastasis rates, with current treatments leading to significant complications like bone defects and infections.

Rationale for the Study

This study aims to develop a multifunctional scaffold using chitosan, black phosphorus nanoparticles, and copper ions in a biphasic calcium phosphate matrix to enhance bone regeneration, reduce tumor recurrence, and prevent infections after osteosarcoma surgery.

Material and Methods

Reagents

CS (90%, 100 kDa) was obtained from Aladdin Biochemical Technology Co., LTD (Shanghai, China). GP and Acetic acid glacial (A.R.) were provided by Linchuan Zhixin Bio-Technology Co., Ltd. (Jiangxi, China). BP dispersion (0.2 mg/mL, transverse dimension: 0.1-5.0 μm) was provided by Nanjing MKNANO Tech. Co., Ltd. (Jiangsu, China). The $CuCl_2$•H_2O (A.R.) were purchased from Kelong Chemical Co., Ltd. (Sichuan, China). Biphase calcium phosphate scaffolds (BCPs) were purchased from Sichuan University. Reverse-osmosis water was used in all experiments.

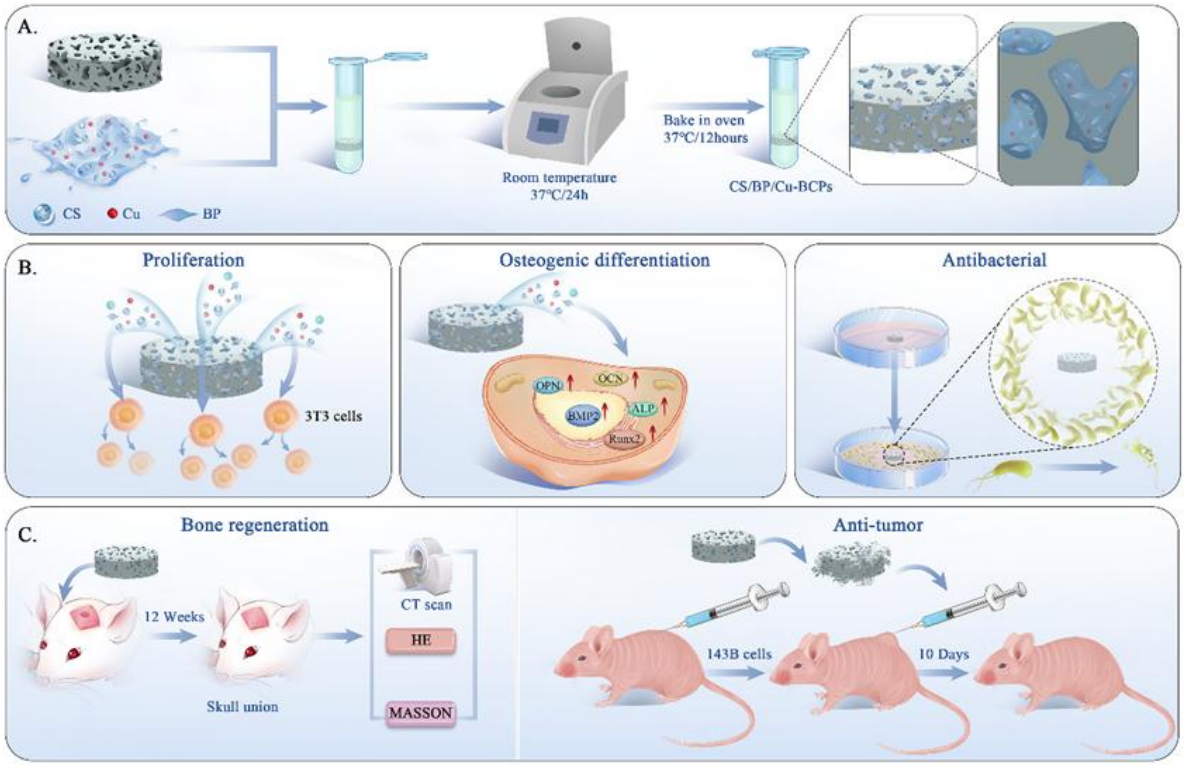

Figure 1. The flow chart of the experiment. (A) Preparation of composite scaffolds; (B) Evaluation of biological function of composite scaffolds *in vitro*; (C) Evaluation of biological function of composite scaffolds *in vivo*.

Fabrication of composite scaffold

The composite scaffolds were fabricated by centrifugation technique and in situ crosslinking method. Briefly, solution A and solution B were prepared, respectively. Solution A: 200 mg CS (20 mg/mL) was mixed with acetic acid solution (1%), and 4 mL BP dispersion and 0.2 mg/mL Cu^{2+} were added after the CS was completely dissolved. Solution B: 100 mg of GP was mixed with 10 mL of RO water and stirred in an indoor environment (25 °C) until completely dissolved. Centrifugation technique and in situ crosslinking: solution B and solution A were added to the centrifuge tube at a volume ratio of 1:10, quickly mix well, and take 0.3 mL of the mixed solution was taken into a 1.5 mL centrifuge tube. A 1.5 mL centrifuge tube was placed in a BCPs scaffold and centrifuged (5000 rpm, 1 min), and then cross-linked at 37 °C for more than 2 h. Therein, the composite scaffold without BP and Cu^{2+} were defined as the CS/BCPs, and the CS/BP/Cu/BCPs without Cu^{2+} were defined as the CS/BP/BCPs.

Characterization of composite scaffolds

Field emission-scanning electron microscopy (FE-SEM, Zeiss Gemini 300, Germany) with an energy-dispersive X-ray spectroscopy was used to observe morphologies and element distribution. The phases were analyzed by X-ray diffraction (XRD, Empyrean, Britain. Range of 2θ: 10° to 80°. Step width: 0.02°). The phases of the samples were analyzed by the Jade 7.0 software (USA). Fourier transform infrared spectroscopy (FTIR, Nicolet 5700, USA) was employed to detect chemical functional groups. Additionally, the compressive modulus was measured using a universal testing machine (Instron-5567, USA).

The evaluation of biocompatibility in vitro

To evaluate the biocompatibility of the composite scaffold, we co-cultured α-MEM medium containing scaffold ion extracts with pre-osteoblast MC3T3-E1. The cells were plated in a 48-well plate at a density of 8000 cells per well, and 300 μL of complete medium was added for overnight incubation. Following the discard of the initial medium, the wells were rinsed twice with PBS. Subsequently, 300

μL/well of ion extract medium was used to culture MC3T3-E1, and the plates were put into a culture incubator for three days (37°C, 5% CO_2). Post-incubation, cell viability was assessed using Alamar Blue reagent, and absorbance was tasted by a microplate reader (λ = 570/600 nm). Pure medium was used as the negative control, while cells cultured with the complete medium served as the positive control. The above procedure was repeated four times.

Antimicrobial evaluation

To evaluate the antibacterial efficacy, 2 mL of bacterial solution (1×10^6CFU/mL) was added into an EP tube, thoroughly mixed with 20 mg of sterile CS/BP/Cu-BCPs powder, and then put into a bacterial incubator for one day. A PBS bacterial solution of equivalent concentration was used as the positive control. Post-incubation, 150 μL of the bacterial suspension was added into a 96-well plate, and the OD value was tested with a microplate reader (λ = 600 nm). The same experimental protocol was employed for Staphylococcus aureus.

For the solid culture assay, 20 μL of bacterial solution (1×10^6CFU/mL) was spread onto bacterial solid culture dishes. Various samples, including BCPs, CS-BCPs, CS/BP-BCPs, and CS/BP/Cu-BCPs, were placed on the solid culture plates and put into a bacterial incubator for one day. After culture, the inhibition zones were documented. The experimental procedure of *S. aureus* was conducted as above. The above procedure was repeated four times.

Evaluation of osteogenic differentiation in vitro

The RNA of BMSCs was extracted by the TRIzol reagent. The concentration and purity of the RNA were assessed by measuring the absorbance ratio at 260 nm and 280 nm. The real-time quantitative polymerase chain reaction (RT-qPCR) was adopted to quantify the relative RNA expression levels, with β-catenin serving as the reference gene. Amplifications were carried out in a final reaction volume of 20.0 μL, with the specific primer sequences. SYBR Green Master Mix (Yeason, 11201ES03, China) was utilized for the amplification, which was conducted over 50 cycles. The relative RNA expression levels were determined using the $2^{-\Delta\Delta Ct}$ method. Each experimental protocol was conducted three times independently to guarantee reproducibility and minimize experimental variation.

After 2 weeks of culturing, the cells were washed three times with PBS, then fixed with 4% paraformaldehyde for 15 minutes. Following fixation, the cells were rinsed three times with deionized water.0.2% Alizarin Red solution was used to stain for 20 min (0.25 mL). The dye solution was discarded, and the cells were rinsed thrice with deionized water. To prevent the wells from drying, an adequate amount of distilled water was added to each well. The cells were imaged and recored using a fluorescence microscope (CKX53, Olympus).

Evaluation of anti-tumor in vivo

143B were injected subcutaneously into the armpit of BALB/c (Nude mice:3-4 weeks old, approximately 15 g in weight) with a concentration of 1×10^7 cells, the injection volume was 100 μL. The above experimental steps were conducted at the Chengdu Third People's Hospital (2022EC1-005). When the tumors reached approximately 10 mm^3, peri-tumoral injections were administered to the mice. The injection of 200μLPBS was used as the control group, while the experimental groups received 100 μL of a 50 mg/mL physiological saline solution mixed with the respective samples. Treatments were administered every three days, and changes in body weight and tumor volume were recorded. The groups included the control group, BCPs, CS-BCPs, CS/BP-BCPs, and CS/BP/Cu-BCPs, with four mice per group.

After eight days of administration, the nude mice were euthanized, and the kidneys, hearts, spleens, lungs, livers, and tumor tissues were harvested. These tissues underwent dehydration, paraffin embedding, sectioning, and staining. Fresh organs were fixed by immersion in a 4% paraformaldehyde solution for 72 h. Fixed tissues were rinsed in distilled water for 2 h, then dehydrated through a graded ethanol series, and finally cleared in xylene. After dehydration, the

tissues were embedded in paraffin, sectioned into ultra-thin slices, and then stained through hematoxylin and eosin (H&E). The sections were treated with xylene, rehydrated through ethanol, and processed with graded ethanol before staining.

Evaluation of bone regeneration in vivo

Female Sprague Dawley (~200g) rats (Dashuo, China) were raised in an animal house free of specific pathogens. After 7 days of acclimation, pentobarbital sodium (2%, 40 mg/kg) was injected intraperitoneally for general anesthesia. A cylindrical critical defect with Φ5mm×1mm was established in the skull with a drill. The rats were divided into the following groups: blank group, BCPs, CS-BCPs, CS/BP-BCPs, and CS/BP/Cu-BCPs. After 4 weeks and 12 weeks, the animals were euthanasia with excessive anesthesia, and the skulls were harvested and fixed with 4% paraformaldehyde solution for further characterizations, include micro-computed tomography (Micro-CT) analysis, hematoxylin-eosin staining (H&E), and Masson staining for in vivo evaluation.

Statistical analysis

All data were presented as mean ± standard deviation (SD). One-way ANOVA and a Tukey multiple comparison test were used to discern the statistical difference between groups. Data were processed using SPSS software when $p < 0.05$ was considered to be statistically significant.

Results

The characterization of composite scaffolds

The findings of this study align with and extend the existing literature on composite scaffolds for bone regeneration. The morphologies of the composite scaffolds, shown in Figure 2A, demonstrate the successful use of porous biphasic calcium phosphates (BCPs) with macro-pore sizes ranging between 250 μm and 500 μm. This range has been highlighted in previous studies, such as by Karageorgiou and Kaplan (2005), which underscore the importance of macro-pore sizes for capillary growth and new bone tissue formation. Our results further support these findings, reinforcing the notion that scaffold porosity plays a crucial role in enhancing vascularization and osteogenesis.

After the incorporation of the composite gel via centrifugation, the filling of BCP pores was confirmed by energy dispersive spectroscopy (EDS), which detected carbon (C) and nitrogen (N) evenly distributed within the scaffold (Figure 2B). This is consistent with the work of Duong *et al.* (2018), who demonstrated the effectiveness of incorporating chitosan in scaffolds to enhance mechanical properties and biological activity. However, while our study shows uniform distribution of copper elements in the CS/BP/Cu-BCPs, the overlapping EDS signals for phosphorus from both black phosphorus (BP) and BCPs indicate a need for further experimental validation to confirm BP's uniform distribution. This challenge has also been noted in studies utilizing similar composite materials (Ma *et al.*, 2022), emphasizing the complexity of accurately characterizing multi-component scaffolds.

X-ray diffraction (XRD) results in Figure 2C indicate that the primary phase of the scaffolds consists of BCPs, with characteristic peaks for both β-Tricalcium phosphate (β-TCP) and hydroxyapatite (HA). These findings are consistent with previous research by Bohner *et al.* (2020) and Maqbool *et al.* (2021), who reported similar XRD patterns confirming the presence of these phases in calcium phosphate-based scaffolds. The successful synthesis of BCPs in our study corroborates these established findings.

Moreover, the infrared spectra in Figure 2D reveal characteristic absorption peaks for phosphate groups in HA, alongside peaks attributed to chitosan (CS), such as the vibration peak at 1076 cm^{-1} for -C-N- and the peak at 1029 cm^{-1} for -C-O-C-. These observations align with the findings of Zhang *et al.* (2018), who also documented the incorporation of chitosan into calcium phosphate scaffolds, indicating that CS enhances both mechanical and biological properties. The findings of our study confirm and expand upon previous research regarding the development of composite scaffolds for bone regeneration. The effective integration of materials such as CS, BP, and copper ions in a biphasic calcium phosphate matrix supports the scaffold's potential in promoting bone healing while

preventing tumor recurrence. Future studies should focus on addressing the challenges of component characterization, particularly the distribution of BP, to optimize scaffold design further. By comparing our results with existing literature, we reinforce the significance of scaffold properties in enhancing bone regeneration and improving clinical outcomes in osteosarcoma management.

.

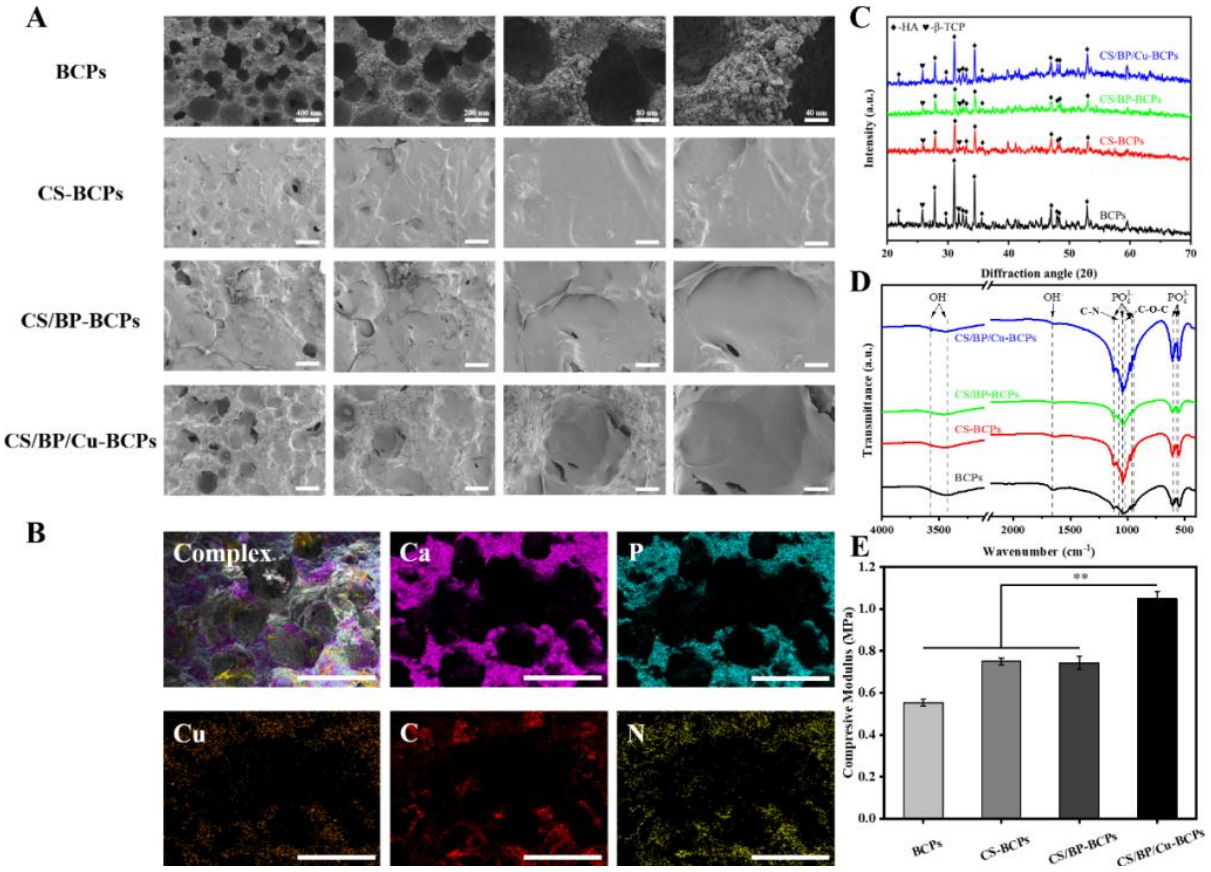

Figure 2. The characterization of composite scaffolds. (A). SEM images, (B). EDS spectrum of CS/BP/Cu/BCPs, Scale bar: 500 μm, C. XRD spectra, D. FTIR spectra, E. Compressive modulus. (n= 3)

The composite scaffold must bear loads to effectively support normal bone tissue. As shown in Figure 2E, the compressive modulus of each group of scaffolds was assessed. Among these, the biphasic calcium phosphate (BCP) scaffold exhibited the lowest compressive modulus at 0.54 MPa, primarily due to its inherent brittleness, which limits deformation under load. According to Feng *et al.* (2022), a compressive strength exceeding 0.5 MPa is sufficient for bone repair scaffolds. The incorporation of organic components into the inorganic BCP scaffold resulted in an increased compressive modulus for the CS-BCPs, CS/BP-BCPs, and CS/BP/Cu-BCPs scaffolds. The formation of an organic cross-linking network significantly improved the toughness of the original BCP scaffold, enhancing its compressive modulus (Shi *et al.*, 2022). Specifically, the compressive moduli of the CS-BCPs and CS/BP-BCPs were measured at 0.73 MPa and 0.72 MPa, respectively, both of which are lower than that of the CS/BP/Cu-BCPs, which reached 1.07 MPa. This increase can be attributed to the introduction of Cu^{2+}, which enhances the cross-linking degree of the organic components and further improves the compressive modulus of the composite scaffold. These findings indicate that the incorporation of both organic materials and copper ions not only improves the mechanical properties of the scaffolds but also aligns with the requirements for effective bone repair, supporting their potential for clinical applications in osteosarcoma management.

The evaluation of biocompatibility in vitro

Herein, the biocompatibility of the scaffolds was assessed by co-culturing MC3T3-E1 cells with extracts of composite scaffolds, with results shown in Figure 3. At three time points, the OD values of cells in all material groups were higher than those in the control group, showing that none of the scaffold groups exhibited cytotoxicity. The excellent biocompatibility of BCPs (Biphasic Calcium Phosphates) and CS has been extensively confirmed by numerous studies (Thangavelu *et al.*, 2020; Duong *et al.*, 2018; Tang *et al.*, 2016). Additionally, the OD values of cells in all groups increased over time. The addition of Cu^{2+} and BP has been demonstrated to promote the proliferation of MC3T3-E1 (Jeon *et al.*, 2021; Li *et al.*, 2019). The results of live/dead staining showed that all groups had a significant number of green live cells, with very few dead cells in each group. Moreover, the density of live cells was lowest in the control group, while it was highest in the CS/BP/Cu-BCPs group, possibly due to the proliferation-promoting effect of copper ions at appropriate concentrations. The results of the cell viability assays and live/dead staining indicate that all groups of scaffolds possess good biocompatibility.

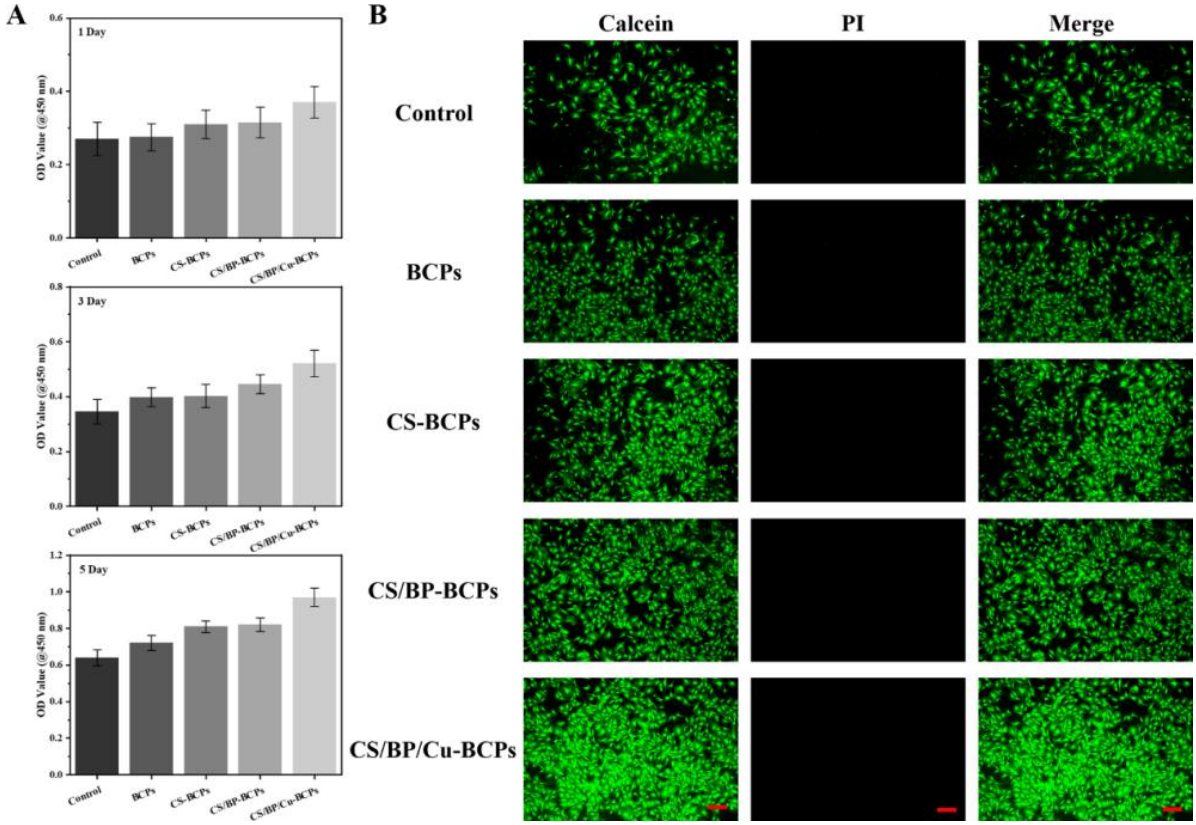

Figure 3. The evaluation of biocompatibility of composite scaffolds *in vitro*. (A) The OD value of MC3T3-E1cellsafter culturing with the ion extract for 1, 3, and 5 days. (B) The live/dead staining images of MC3T3-E1cells after co-culturing with composite scaffolds for 5 days. (n= 3)

The evaluation of antimicrobial activity in vitro

Bacterial infections can trigger inflammatory responses, hindering the normal bone tissue repair process. To evaluate the tolerance of *Escherichia coli* (E. coli) and *Staphylococcus aureus* (S. aureus) to the different scaffold groups, co-culture and plate counting methods were employed, with results presented in Figure 4. Antibacterial performance against both bacterial strains was assessed through suspension experiments and the inhibition zone method, as shown in Figure 4A.

All experimental scaffold groups exhibited notable antibacterial properties against *E. coli* and *S. aureus*. However, a significant enhancement in antibacterial performance was observed with the

incorporation of chitosan (CS). Previous studies have indicated that CS possesses excellent antibacterial properties against a variety of bacterial strains (Liang *et al.*, 2021; Song *et al.*, 2021).

While black phosphorus (BP) has been identified as an effective antibacterial agent capable of combating bacterial antibiotic resistance through the generation of reactive oxygen species (ROS) and oxidative stress (Aksoy *et al.*, 2020; Liu *et al.*, 2020), our experiments suggested that BP's antibacterial efficacy was not fully realized within the scaffold. This limitation may be attributed to the short lifespan and restricted action distance of ROS in this context. Nevertheless, the addition of copper ions (Cu^{2+}) significantly enhanced the overall antibacterial performance.

Among all scaffold groups, the CS/BP/Cu-BCPs exhibited the most substantial inhibitory effects on both bacterial strains, as illustrated in Figures 4A and 4B. The observed antibacterial activity can be partially explained by the interaction of CS with bacterial cell walls, leading to cell wall disruption and subsequent bacterial death. Furthermore, the incorporation of Cu^{2+} likely contributes to this effect by binding with phospholipids in the bacterial membrane, causing membrane disruption and leakage of intracellular contents (Dadi *et al.*, 2019; Kaweeteerawat *et al.*, 2015; Shi *et al.*, 2023).

Overall, the design of this composite scaffold demonstrates excellent antibacterial activity, showcasing significant potential for infection control in clinical applications related to bone repair and osteosarcoma management.

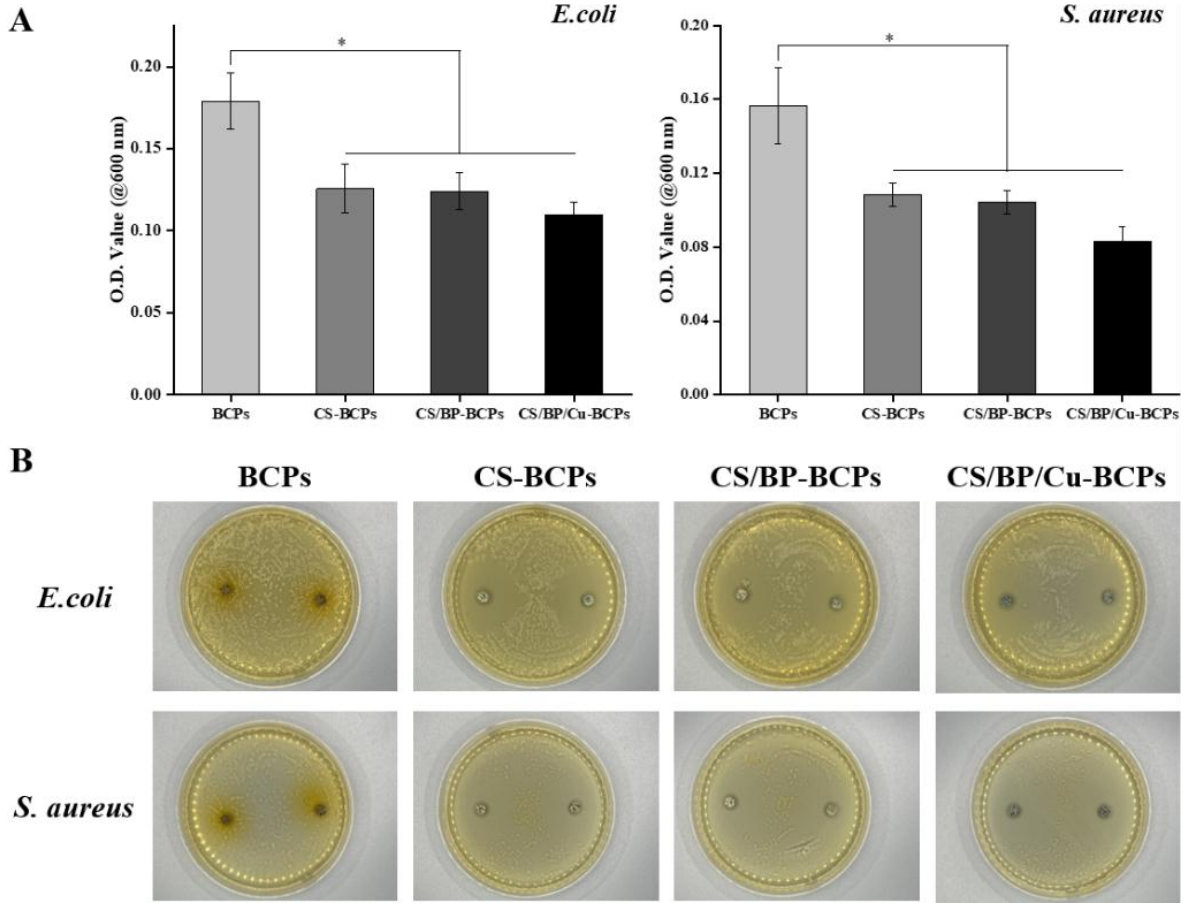

Figure 4. The evaluation of the antibacterial performance of composite scaffolds in vitro. (A) The OD value of *E. coli* and *S. aureus* after culturing with composite scaffolds for 24 h, (B) The colony results after co-cultivation of the composite scaffolds with *E. coli* and *S. aureus* for 24 h. (n= 3)

The osteogenic differentiation potentialin vitro

To validate the in vitro osteogenic differentiation potential of composite scaffolds, BMSCs were cultured with the extracts of composite scaffolds for 14 days. The expression of genes and proteins

related to osteogenic differentiation (OPN, BMP-2,OCN, RUNX2,and ALP) was then examined, as depicted in Figure 5.

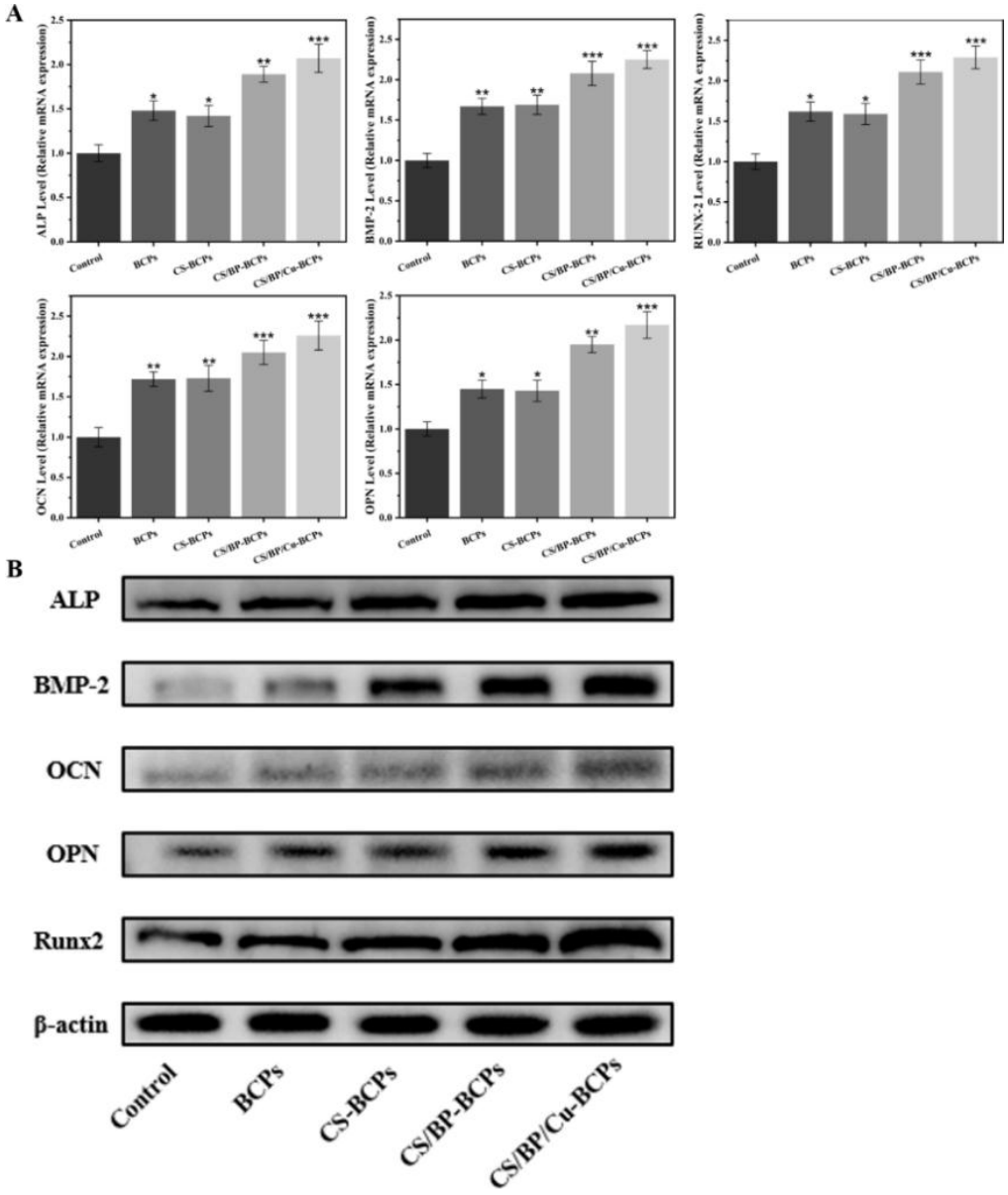

Figure 5. The evaluation of osteogenic differentiation of composite scaffolds in vitro. (A) Osteogenesis-related genes in BMSCs including ALP, BMP-2, OCN, OPN, and Runx2 at 14 days, (B) Western blot images of ALP, BMP-2, OCN, OPN, and Runx2 after culturing for 14 days. (n= 3)

The results revealed a significantly higher expression of osteogenesis-related genes in the experimental group compared to the control group, indicating that BCPs can markedly promote osteogenic differentiation of BMSCs. The osteogenic effects of BCPs have been well-established in numerous studies (Bouler *et al.*, 2017). However, the expression levels of osteogenesis-related genes in BCPs and CS-BCPs were similar, suggesting that the addition of CS did not significantly enhance the osteogenic promotion effect of BCPs. BCP particles could significantly improve the in vitro osteogenic promotion effect of the porous chitosan scaffold, while a pure chitosan scaffold showed no significant difference in osteogenic promotion relative to the control group (Sendemir-Urkmez *et al.*, 2007). Upon the supplementation of BP, the expression levels of osteogenesis-related genes in CS/BP-BCPs were significantly improved, indicating that BP has a notable osteogenic promotion effect (Ma *et al.*, 2022). Of course, the expression levels of osteogenesis-related genes in CS/BP/Cu-

BCPs were the highest, attributed to the synergistic osteogenic promotion effect of BCPs, BP, and Cu^{2+}. Cu^{2+} not only promotes osteogenesis but also exhibits significant effects in inducing vascular regeneration and antibacterial functions. Vascular ingrowth plays a crucial role in the subsequent bone tissue growth process (Rivera *et al.*, 2021). Cu^{2+} can significantly improve the vascularization and osteogenic effects of Calcium Phosphates (CaPs) (Xiao *et al.*, 2018). The expression of osteogenesis-related proteins was also assessed, as shown in Figure 5B. The results indicated that the expression of osteogenesis-related proteins paralleled the expression of genes, with higher expression levels in the experimental group compared to the control group. The osteogenic promotion effect of BCPs was improved with the addition of BP and Cu^{2+}. The highest expression levels were observed in CS/BP/Cu-BCPs. BP can promote the expression of ALP, OCN, and Runx2 in BMSCs (Ma *et al.*, 2022). Cu^{2+} not only elevates the secretion of ALP, Runx2, Col-I, and OCN in BMSCs but also enhances the expression of VEGF and NO in endothelial cells, further improving the in vitro osteogenic differentiation effect of CaPs (Lin *et al.*, 2020). Quantitative statistical analysis of immunoblotting grayscale values yielded results consistent with those shown in Figure 5B, as illustrated in Figure S1. In summary, the *in vitro* osteogenic differentiation experiments suggest that BCPs exhibit a significant osteogenic promotion effect, whereas the effect of CS is suboptimal, and the addition of BP and Cu^{2+} can significantly enhance the osteogenic promotion effect of BCPs.

The evaluation of anti-tumor in vivo

The *in vivo* antitumor effects of composite scaffolds were appraised by measuring the size of tumor tissues in nude mice after administration, as shown in Figure 6A.

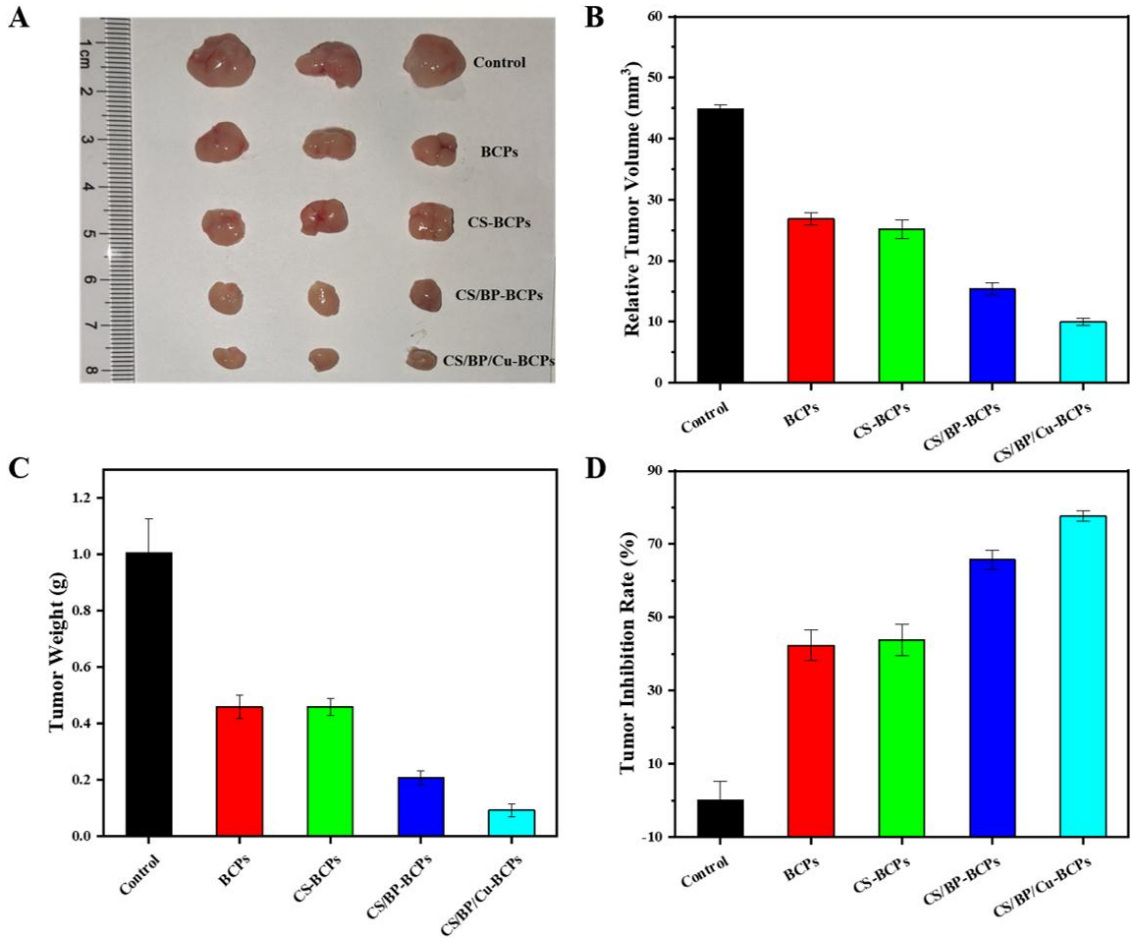

Figure 6. The antitumor effect of composite scaffolds *in vivo*. (A) Photographs of tumor tissue. (B) Relative tumor volume, (C) Tumor weight, (D) Tumor inhibition rate.

The tumor size of the control group was the largest, while that of the BCPs was slightly smaller than the control group but not notably inhibited. The antitumor effect of BCPs was due to their dissolution in the low pH environment of the tumor, releasing a substantial amount of Ca^{2+}, which leads to tumor cell apoptosis (Wu *et al.*, 2024). The CS-BCPs group demonstrated a similar antitumor mechanism to the BCPs group, demonstating that the supplement of CS did not markedly improve the antitumor effect of BCPs. The CS/BP-BCPs and CS/BP/Cu-BCPs displayed better antitumor effects than the control groups, BCPs, and CS-BCPs, which attributed to the excellent antitumor properties of BP and Cu^{2+}(Song *et al.*, 2023; Yang *et al.*, 2018). Pan *et al.*'s study employed in situ calcium phosphate (CaP) mineralization to enhance BP's anticancer activity. Compared to BP, Ca-BP exhibited enhanced anticancer bioactivity due to improved pH-responsive degradation and intracellular Ca^{2+} overload in cancer cells(Pan *et al.*, 2020). Copper-loaded chitosan nanoparticles demonstrated stronger inhibitory effects on osteosarcoma than pure chitosan nanoparticles(Ai *et al.*, 2017). CS/BP/Cu-BCPs showed the smallest tumor size, indicating a significant synergistic antitumor effect of BP and Cu^{2+}. Quantitative analysis of tumor volume, tumor size, and inhibition rate consistently showed superior antitumor effects in the material groups compared to the control group, as shown in Figure 6 (B-D). CS/BP-BCPs and CS/BP/Cu-BCPs exhibited more pronounced antitumor effects. CS-BCPs slightly outperformed BCPs, attributed to CS's antitumor activity(Dana *et al.*, 2021). The study of Koski *et al.* (2020) has demonstrated that CS-loaded hydroxyapatite tablets significantly inhibit the activity of osteosarcoma cells after 6 days of co-culture with osteosarcoma cells compared to pure hydroxyapatite (Koski *et al.*, 2020). The optimal antitumor efficacy of CS/BP/Cu-BCPs is attributed to the synergistic action of overloaded Cu^{2+}, BP, and CS. In conclusion, *in vivo* antitumor results demonstrated that the multifunctional gel could enhance the in vivo antitumor efficacy of BCPs.

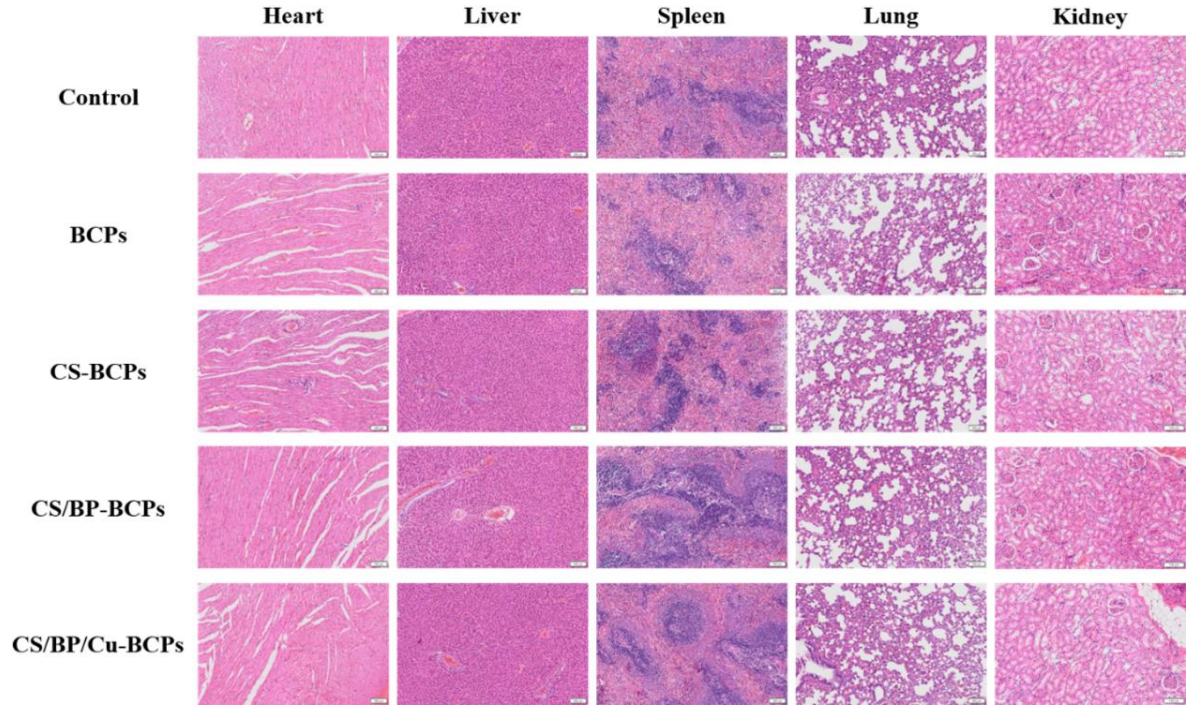

Figure 7. H&E staining of the heart, liver, spleen, lung, and kidney after the mice were sacrificed; scale bar: 100 μm.

The evaluation of biological safety

The heart, liver, spleen, lung, and kidney tissues of nude mice were subjected to Hematoxylin and Eosin (H&E) staining to evaluate the biosafety of composite scaffolds, as shown in Figure 7. The H&E staining showed no significant lesions in the major organs and revealed no significant histopathological changes in all groups, which indicated that all scaffolds caused no damage to the major organs of the mice, confirmed the biosafety of composite scaffolds for *in vivo* antitumor therapy.

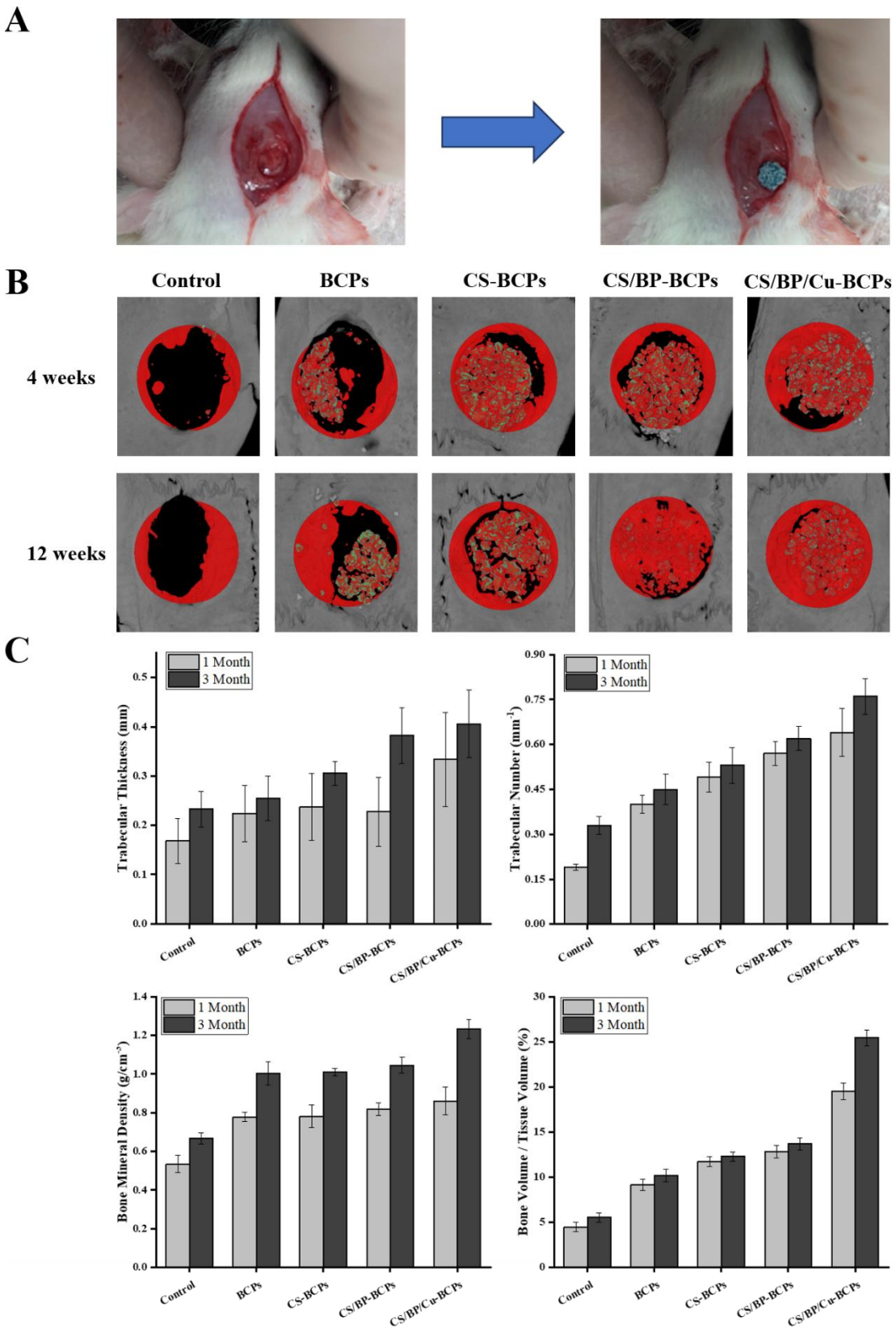

Figure 8. The evaluation results of bone repair with composite scaffolds implanted for 4 and 12 weeks. (A) Bone defect reconstruction filling diagram, (B) Micro-CT, (C) Trabecular thickness, trabecular number, bone mineral density results, and bone volume/total volume. (n= 3) results of CT and mineralization density.

The evaluation of bone repair in vivo

SD rats cranial defect modeling was selected for evaluating the osteogenesis efficacy of the composite scaffolds, as shown in Figure 8A. After 4 weeks and 12 weeks of implantation, Micro-CT, Masson staining, and H&E were adopted to examine the mediation effect. As depicted in Figure 8B, only a little bone tissue grew into the defect of the control group due to the absence of any bioactive material implantation, with no significant new bone formation observed even after 12 weeks. In contrast, the scaffold groups could induce more bone tissue to grow into the defect site, with the areas of bone formation progressively increasing in the BCPs, CS-BCPs, CS/BP-BCPs, and CS/BP/Cu-BCPs. Biphasic calcium phosphate could repair large bone defects, but its ability to induce angiogenesis was poor (Rustom *et al.*, 2016).

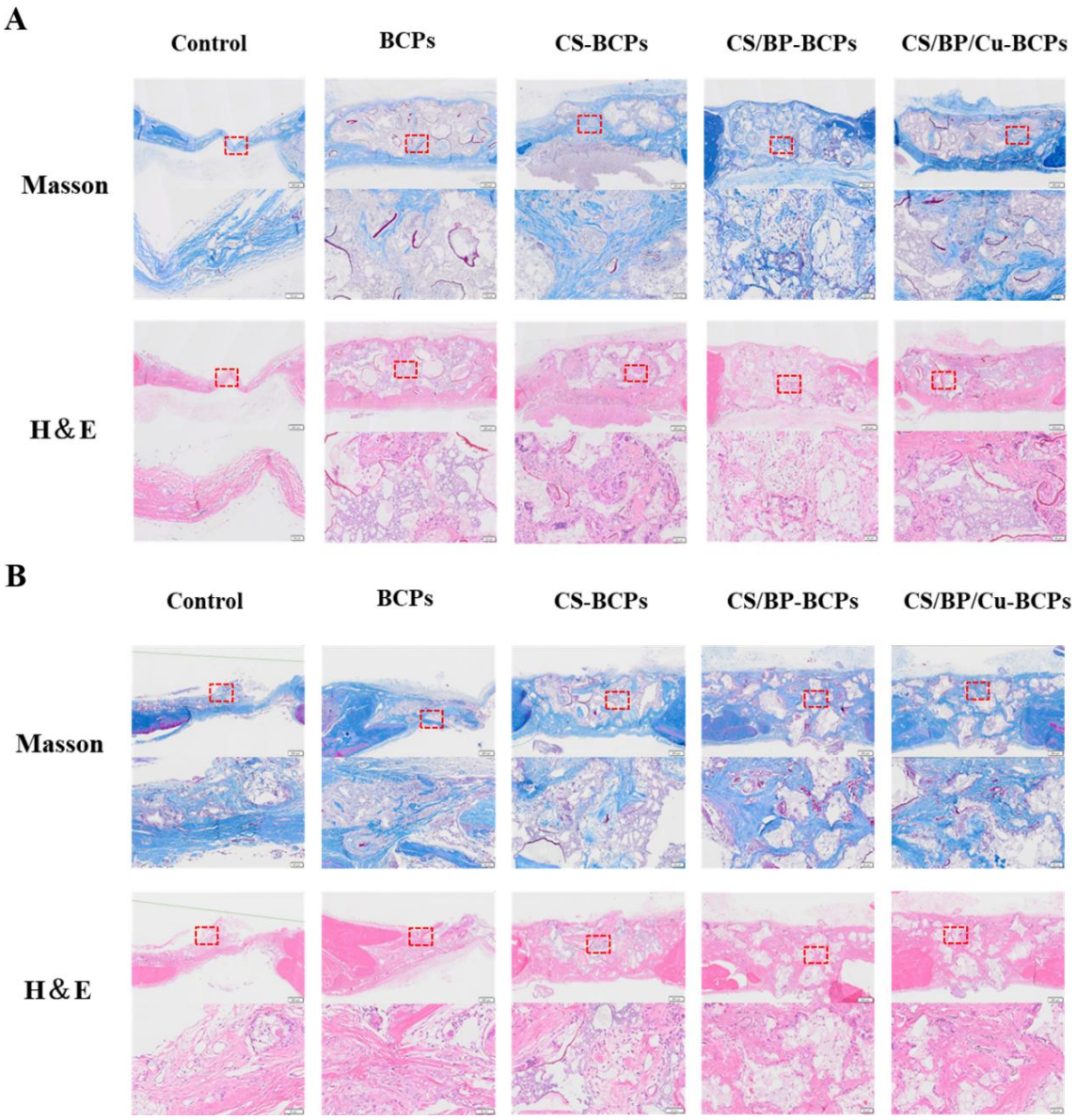

Figure 9. The result of the H&E and Masson staining. (A) 4 weeks; (B) 12weeks. Scale bar:200 μm, and the enlarged area scale bar: 50 μm. (n= 3)

The results of bone mineral density followed a similar trend to the bone formation area; the values of BCPs, CS-BCPs, and CS/BP-BCPs all higher than the control group, and CS/BP/Cu-BCPs displayed the highest values. Regarding the bone volume to tissue volume ratio, the control group was the lowest, followed by increasing values in the BCPs, CS-BCPs, and CS/BP-BCPs, which may be attributed to the osteogenic effect of BCPs, while CS has little effect on osteogenesis. A chitosan

coating could not significantlyimprove the osteogenic effect of BCP scaffolds (Fan *et al.*, 2022). Furthermore, the values for CS/BP-BCPs are higher than BCPs and CS-BCPs, indicating that BP has a superior bone-promoting effect. The enhanced osteogenic effect of calcium phosphate with BP has been confirmed in related studies(Ma *et al.*, 2022). The CS/BP/Cu/BCPs group had the highest bone-to-tissue volume ratio, which was due to the combined promotive effects of BCPs, BP, and Cu^{2+} on bone regeneration. Cu^{2+} can improve the osteogenic effect of calcium phosphate (Lin *et al.*, 2020; Zhang *et al.*, 2016).The results of trabecular thickness and number consistently increased in the control, BCPs, CS-BCPs, CS/BP-BCPs, and CS/BP/Cu-BCPs, as shown in Figure 9B. The trabecular number statistics was consistent with the results of H&E and Masson staining are shown in Figure 9. The H&E staining showed that the bone repair effects of BCPs, CS-BCPs, CS/BP-BCPs, and CS/BP/Cu-BCPs were superior to those of the control group, with CS/BP/Cu-BCPs demonstrating the best bone repair effect. The result of Masson staining was similar to H&E. H&E and Masson staining results indicate that the multifunctional gel loaded with BP and Cu^{2+} significantly improves the bone-promoting effect of BCPs. He *et al.* (2022) suggests that black phosphorus/chitosan composite coatings markedly enhance the bone-promoting effect of PEEK scaffolds. Related studies show that BCP has the effect of bone induction, and Cu^{2+} can improve the osteogenic effect of BCP (Gomes *et al.*, 2018; Wu *et al.*, 2022). In summary, the *in vivo* bone repair results indicated that the multifunctional gel loaded with BP and Cu^{2+} can improve the *in vivo* osteogenic effect of BCPs.

Conclusion

In this study, we successfully prepared biphasic calcium phosphate porous scaffolds (BCPs) using the pore-forming agent method and infused them with chitosan (CS) gel loaded with copper ions and black phosphorus (BP) nanosheets to create composite scaffolds (CS-BCPs, CS/BP-BCPs, and CS/BP/Cu-BCPs). Our mechanical property tests indicated that the composite scaffolds exhibited enhanced compressive strength compared to the BCPs alone, supporting their potential for load-bearing applications. In vitro biocompatibility evaluations showed that all scaffold groups were well-tolerated, with CS/BP/Cu-BCPs demonstrating the most significant promotion of MC3T3-E1 cell proliferation. Notably, these composite scaffolds exhibited superior antibacterial effects when compared to hydroxyapatite (HA), with the CS/BP/Cu-BCPs showing the highest antibacterial performance against *E. coli* and *S. aureus*. Osteogenic differentiation experiments further revealed that bone marrow stem cells (BMSCs) co-cultured with CS/BP/Cu-BCPs expressed elevated levels of osteogenesis-related genes, indicating robust osteogenic differentiation.

In vivo studies revealed anti-tumor effects for all composite scaffolds, with CS/BP/Cu-BCPs demonstrating the most significant tumor suppression compared to the control group. Additionally, in cranial defect repair experiments, all scaffold types facilitated bone repair, but CS/BP/Cu-BCPs achieved the most effective results, particularly notable after three months of implantation.

Overall, the composite scaffolds developed in this study show considerable promise for clinical applications in promoting new bone formation following osteosarcoma resection. Future research should focus on optimizing the scaffold's mechanical properties and investigating the long-term efficacy of these materials in clinical settings. Additionally, exploring the interactions between the scaffold components and various cell types could further enhance the therapeutic potential of these scaffolds in bone tissue engineering and cancer treatment.

Acknowledgement

Authors are thankful to Lincoln University College management for academic support.

Conflict of Interest

The authors declare no known competing financial interests or personal relationships that may appear to have influenced this study.

References

Ai, J. W., Liao, W., & Ren, Z. L. (2017). Enhanced anticancer effect of copper-loaded chitosan nanoparticles against osteosarcoma. *RSC advances*, 7(26), 15971-15977. https://doi.org/10.1039/c6ra21648j

Aksoy, I., Kucukkececi, H., Sevgi, F., Metin, O., & Hatay Patir, I. (2020). Photothermal antibacterial and antibiofilm activity of black phosphorus/gold nanocomposites against pathogenic bacteria. *ACS applied materials & interfaces*, 12(24), 26822-26831. https://doi.org/10.1021/acsami.0c02524

Bohner, M., Santoni, B. L. G., & Döbelin, N. (2020). β-tricalcium phosphate for bone substitution: Synthesis and properties. *Acta biomaterialia*, 113, 23-41. https://doi.org/10.1016/j.actbio.2020.06.022

Bouler, J. M., Pilet, P., Gauthier, O., & Verron, E. (2017). Biphasic calcium phosphate ceramics for bone reconstruction: A review of biological response. *Acta biomaterialia*, 53, 1-12. https://doi.org/10.1016/j.actbio.2017.01.076

Cheng, R. X., Tian, F. Y., Zhang, Y. Q., Chen, K., Zhu, Q. J., & Tao, Z. (2020). TMeQ [6]-based supramolecular frameworks assembled through outer surface interactions and their potential applications. *Journal of Materials Science*, 55, 16497-16509. https://doi.org/10.1007/s10853-020-05180-7

da Silva, D. A., De Luca, A., Squitti, R., Rongioletti, M., Rossi, L., Machado, C. M., & Cerchiaro, G. (2022). Copper in tumors and the use of copper-based compounds in cancer treatment. *Journal of inorganic biochemistry*, 226, 111634. https://doi.org/10.1016/j.jinorgbio.2021.111634

Dadi, R., Azouani, R., Traore, M., Mielcarek, C., & Kanaev, A. (2019). Antibacterial activity of ZnO and CuO nanoparticles against gram positive and gram negative strains. *Materials Science and Engineering*: C, 104, 109968. https://doi.org/10.1016/j.msec.2019.109968

Dana, P. M., Hallajzadeh, J., Asemi, Z., Mansournia, M. A., & Yousefi, B. (2021). Chitosan applications in studying and managing osteosarcoma. *International journal of biological macromolecules*, 169, 321-329. https://doi.org/10.1016/j.ijbiomac.2020.12.058

Deng, K., Chen, H., Dou, W., Cai, Q., Wang, X., Wang, S., & Wang, D. (2022). Preparation and characterization of porous HA/β-TCP biphasic calcium phosphate derived from butterfish bone. *Materials Technology*, 37(10), 1388-1395. https://doi.org/10.1080/10667857.2021.1950886

Duong, H. V., Chau, T. T. L., Dang, N. T. T., Vanterpool, F., Salmeron-Sanchez, M., Lizundia, E., ... & Nguyen, T. D. (2018). Biocompatible chitosan-functionalized upconverting nanocomposites. *ACS omega*, 3(1), 86-95. https://doi.org/10.1021/acsomega.7b01355

Fan, S., Wan, Y., Zhao, Z., Wang, H., & Ji, Z. (2022). Biological evaluation of polydopamine and chitosan composite coatings on the 3D printed porous biphasic calcium phosphate scaffold. *Ceramics International*, 48(19), 27942-27956. https://doi.org/10.1016/j.ceramint.2022.06.098

Feng, C., Wu, Y., Li, Q., He, T., Cao, Q., Li, X., ... & Zhang, X. (2022). A novel hollow-tube-biphasic-whisker-modified calcium phosphate ceramics with simultaneously enhanced mechanical strength and osteogenic activity. *Advanced Functional Materials*, 32(44), 2204974. https://doi.org/10.1002/adfm.202204974

Gomes, S., Vichery, C., Descamps, S., Martinez, H., Kaur, A., Jacobs, A., ... & Renaudin, G. (2018). Cu-doping of calcium phosphate bioceramics: From mechanism to the control of cytotoxicity. *Acta Biomaterialia*, 65, 462-474. https://doi.org/10.1016/j.actbio.2017.10.028

Haurat, M., Tassaing, T., & Dumon, M. (2022). FTIR in situ measurement of swelling and CO2 sorption in acrylic polymers at high CO2 pressures. *The Journal of Supercritical Fluids*, 182, 105534. https://doi.org/10.1016/j.supflu.2022.105534

He, M., Zhu, C., Sun, D., Liu, Z., Du, M., Huang, Y., ... & Zhang, L. (2022). Layer-by-layer assembled black phosphorus/chitosan composite coating for multi-functional PEEK bone scaffold. *Composites Part B: Engineering*, 246, 110266. https://doi.org/10.1016/j.compositesb.2022.110266

Huang, H., Yang, A., Li, J., Sun, T., Yu, S., Lu, X., ... & Weng, J. (2022). Preparation of multigradient hydroxyapatite scaffolds and evaluation of their osteoinduction properties. *Regenerative Biomaterials*, 9, rbac001. https://doi.org/10.1093/rb/rbac001

Ingley, K. M., Maleddu, A., Grange, F. L., Gerrand, C., Bleyer, A., Yasmin, E., ... & Strauss, S. J. (2022). Current approaches to management of bone sarcoma in adolescent and young adult patients. *Pediatric Blood & Cancer*, 69(2), e29442-e29442. https://doi.org/10.1002/pbc.29442

Jeon, S., Lee, J. H., Jang, H. J., Lee, Y. B., Kim, B., Kang, M. S., ... & Han, D. W. (2021). Spontaneously promoted osteogenic differentiation of MC3T3-E1 preosteoblasts on ultrathin layers of black phosphorus. *Materials Science and Engineering*: C, 128, 112309. https://doi.org/10.1016/j.msec.2021.112309

Kansara, M., Teng, M. W., Smyth, M. J., & Thomas, D. M. (2014). Translational biology of osteosarcoma. *Nature Reviews Cancer*, 14(11), 722-735. https://doi.org/10.1038/nrc3838

Karageorgiou, V., & Kaplan, D. (2005). Porosity of 3D biomaterial scaffolds and osteogenesis. *Biomaterials*, 26(27), 5474-5491. https://doi.org/10.1016/j.biomaterials.2005.02.002

Kaweeteerawat, C., Chang, C. H., Roy, K. R., Liu, R., Li, R., Toso, D., ... & Godwin, H. A. (2015). Cu nanoparticles have different impacts in Escherichia coli and Lactobacillus brevis than their microsized and ionic analogues. *ACS nano*, 9(7), 7215-7225. https://doi.org/10.1021/acsnano.5b02021

Koski, C., Vu, A. A., & Bose, S. (2020). Effects of chitosan-loaded hydroxyapatite on osteoblasts and osteosarcoma for chemopreventative applications. *Materials Science and Engineering:* C, 115, 111041. https://doi.org/10.1016/j.msec.2020.111041

Lazarevic, M., Petrovic, S., Pierfelice, T. V., Ignjatovic, N., Piattelli, A., Vlajic Tovilovic, T., & Radunovic, M. (2023). Antimicrobial and Osteogenic Effects of Collagen Membrane Decorated with Chitosan–Nano-Hydroxyapatite. *Biomolecules*, 13(4), 579. https://doi.org/10.3390/biom13040579

Li, K., Xia, C., Qiao, Y., & Liu, X. (2019). Dose-response relationships between copper and its biocompatibility/antibacterial activities. *Journal of Trace Elements in Medicine and Biology*, 55, 127-135. https://doi.org/10.1016/j.jtemb.2019.06.015

Liang, Y., Li, Z., Huang, Y., Yu, R., & Guo, B. (2021). Dual-dynamic-bond cross-linked antibacterial adhesive hydrogel sealants with on-demand removability for post-wound-closure and infected wound healing. *ACS nano*, 15(4), 7078-7093. https://doi.org/10.1021/acsnano.1c00204

Lin, Z., Cao, Y., Zou, J., Zhu, F., Gao, Y., Zheng, X., ... & Wu, T. (2020). Improved osteogenesis and angiogenesis of a novel copper ions doped calcium phosphate cement. *Materials Science and Engineering*: C, 114, 111032. https://doi.org/10.1016/j.msec.2020.111032

Liu, W., Zhang, Y., Zhang, Y., & Dong, A. (2020). Black phosphorus nanosheets counteract bacteria without causing antibiotic resistance. *Chemistry–A European Journal*, 26(11), 2478-2485. https://doi.org/10.1002/chem.201905134

Luetke, A., Meyers, P. A., Lewis, I., & Juergens, H. (2014). Osteosarcoma treatment–where do we stand? A state of the art review. *Cancer treatment reviews*, 40(4), 523-532. https://doi.org/10.1016/j.ctrv.2013.11.006

Ma, S., Wei, Y., Sun, R., Xu, H., Liu, X., Wang, Y., ... & Huang, D. (2022). Calcium phosphate bone cements incorporated with black phosphorus nanosheets enhanced osteogenesis. *ACS Biomaterials Science & Engineering,* 9(1), 292-302. https://doi.org/10.1021/acsbiomaterials.2c00742

Maqbool, M., Nawaz, Q., Atiq Ur Rehman, M., Cresswell, M., Jackson, P., Hurle, K., ... & Boccaccini, A. R. (2021). Synthesis, characterization, antibacterial properties, and in vitro studies of selenium and strontium co-substituted hydroxyapatite. *International Journal of Molecular Sciences*, 22(8), 4246. https://doi.org/10.3390/ijms22084246

Mir, T. U. G., Shukla, S., Malik, A. Q., Singh, J., & Kumar, D. (2023). Microwave-assisted synthesis of N-doped carbon quantum dots for detection of methyl orange in saffron. *Chemical Papers*, 77(7), 3641-3649. https://doi.org/10.1007/s11696-023-02726-2

Pan, T., Fu, W., Xin, H., Geng, S., Li, Z., Cui, H., ... & Yu, X. F. (2020). Calcium phosphate mineralized black phosphorous with enhanced functionality and anticancer bioactivity. *Advanced Functional Materials*, 30(38), 2003069. https://doi.org/10.1002/adfm.202003069

Qiu, M., Singh, A., Wang, D., Qu, J., Swihart, M., Zhang, H., & Prasad, P. N. (2019). Biocompatible and biodegradable inorganic nanostructures for nanomedicine: silicon and black phosphorus. *Nano Today*, 25, 135-155. https://doi.org/10.1016/j.nantod.2019.02.012

Ritter, J., & Bielack, S. S. (2010). Osteosarcoma. Annals of oncology, 21, vii320-vii325. https://doi.org/10.1093/annonc/mdq276

Rivera, L. R., Cochis, A., Biser, S., Canciani, E., Ferraris, S., Rimondini, L., & Boccaccini, A. R. (2021). Antibacterial, pro-angiogenic and pro-osteointegrative zein-bioactive glass/copper based coatings for implantable stainless steel aimed at bone healing. *Bioactive materials*, 6(5), 1479-1490. https://doi.org/10.1016/j.bioactmat.2020.11.001

Rustom, L. E., Boudou, T., Lou, S., Pignot-Paintrand, I., Nemke, B. W., Lu, Y., ... & Johnson, A. J. W. (2016). Micropore-induced capillarity enhances bone distribution in vivo in biphasic calcium phosphate scaffolds. *Acta biomaterialia*, 44, 144-154. https://doi.org/10.1016/j.actbio.2016.08.025

Sanuki-Fujimoto, N., Takeda, A., Amemiya, A., Ofuchi, T., Ono, M., Yamagami, R., ... & Shigematsu, N. (2008). Pattern of tumor recurrence in initially nonmetastatic breast cancer patients: distribution and frequency of metastases at unusual sites. Cancer: *Interdisciplinary International Journal of the American Cancer Society*, 113(4), 677-682. https://doi.org/10.1002/cncr.23612

Sendemir-Urkmez, A., & Jamison, R. D. (2007). The addition of biphasic calcium phosphate to porous chitosan scaffolds enhances bone tissue development in vitro. *Journal of Biomedical Materials Research Part* A, 81(3), 624-633. https://doi.org/10.1002/jbm.a.31010

Shi, C., Hou, X., Zhao, D., Wang, H., Guo, R., & Zhou, Y. (2022). Preparation of the bioglass/chitosan-alginate composite scaffolds with high bioactivity and mechanical properties as bone graft materials. *Journal of the Mechanical Behavior of Biomedical Materials*, 126, 105062. https://doi.org/10.1016/j.jmbbm.2021.105062

Shi, Y., Li, Y., Huang, C., Xu, Y., & Xu, Y. (2023). Electrogenerated copper selenide with positive charge to efficiently capture and combat drug-resistant bacteria for wound healing. *Journal of Colloid and Interface Science*, 634, 852-863. https://doi.org/10.1016/j.jcis.2022.12.094

Song, H. Q., Fan, Y., Hu, Y., Cheng, G., & Xu, F. J. (2021). Polysaccharide–peptide conjugates: a versatile material platform for biomedical applications. *Advanced Functional Materials*, 31(6), 2005978. https://doi.org/10.1002/adfm.202005978

Song, H., Ji, Y., Zhu, Y., Xia, J., Hu, C., Jin, Y., ... & Dai, J. (2023). One-pot synthesized nano-heterostructure with dual-modal catalytic ROS generation ability for high-metastatic orthotopic osteosarcoma therapy. *Carbon*, 204, 196-210. https://doi.org/10.1016/j.carbon.2022.12.053

Tang, X., Mao, L., Liu, J., Yang, Z., Zhang, W., Shu, M., ... & Fang, B. (2016). Fabrication, characterization and cellular biocompatibility of porous biphasic calcium phosphate bioceramic scaffolds with different pore sizes. *Ceramics International*, 42(14), 15311-15318. https://doi.org/10.1016/j.ceramint.2016.06.172

Thangavelu, M., Adithan, A., Peter, J. S. J., Hossain, M. A., Kim, N. S., Hwang, K. C., ... & Kim, J. H. (2020). Ginseng compound K incorporated porous Chitosan/biphasic calcium phosphate composite microsphere for bone regeneration. *International journal of biological macromolecules*, 146, 1024-1029. https://doi.org/10.1016/j.ijbiomac.2019.09.228

Waibel, K. H., Haney, B., Moore, M., Whisman, B., & Gomez, R. (2011). Safety of chitosan bandages in shellfish allergic patients. *Military medicine*, 176(10), 1153-1156. https://doi.org/10.7205/MILMED-D-11-00150

Wu, J., Feng, C., Wang, M., Wu, H., Zhu, X., Li, X., ... & Zhang, X. (2022). Whisker of biphasic calcium phosphate ceramics: Osteo-immunomodulatory behaviors. *Nano Research*, 15(10), 9169-9182. https://doi.org/10.1007/s12274-022-4591-0

Wu, Y., Cheng, M., Jiang, Y., Zhang, X., Li, J., Zhu, Y., & Yao, Q. (2024). Calcium-based biomaterials: Unveiling features and expanding applications in osteosarcoma treatment. *Bioactive Materials*, 32, 385-399. https://doi.org/10.1016/j.bioactmat.2023.10.008

Xiao, D., Yang, F., Zhao, Q., Chen, S., Shi, F., Xiang, X., ... & Feng, G. (2018). Fabrication of a Cu/Zn co-incorporated calcium phosphate scaffold-derived GDF-5 sustained release system with enhanced angiogenesis and osteogenesis properties. *RSC advances*, 8(52), 29526-29534. https://doi.org/10.1039/c8ra05441j

Yang, B., Yin, J., Chen, Y., Pan, S., Yao, H., Gao, Y., & Shi, J. (2018). 2D-black-phosphorus-reinforced 3D-printed scaffolds: a stepwise countermeasure for osteosarcoma. *Advanced Materials*, 30(10), 1705611. https://doi.org/10.1002/adma.201705611

Yao, G., Lei, J., Zhang, W., Yu, C., Sun, Z., Zheng, S., & Komarneni, S. (2019). Antimicrobial activity of X zeolite exchanged with Cu 2+ and Zn 2+ on Escherichia coli and Staphylococcus aureus. *Environmental Science and Pollution Research*, 26, 2782-2793. https://doi.org/10.1007/s11356-018-3750-z

Zhang, L., Fang, H., Zhang, K., & Yin, J. (2018). Homologous sodium alginate/chitosan-based scaffolds, but contrasting effect on stem cell shape and osteogenesis. *ACS applied materials & interfaces*, 10(8), 6930-6941. https://doi.org/10.1021/acsami.7b18859

Zhang, W., Chang, Q., Xu, L., Li, G., Yang, G., Ding, X., ... & Jiang, X. (2016). Graphene oxide-copper Nanocomposite-coated porous CaP scaffold for vascularized bone regeneration via activation of Hif-1α. *Advanced healthcare materials*, 5(11), 1299-1309. https://doi.org/10.1002/adhm.201500824

Zhou, M., Wu, X., Luo, J., Yang, G., Lu, Y., Lin, S., ... & Jiang, X. (2021). Copper peptide-incorporated 3D-printed silk-based scaffolds promote vascularized bone regeneration. *Chemical Engineering Journal*, 422, 130147. https://doi.org/10.1016/j.cej.2021.130147